USING TRANSVERSE ISOTROPY TO MODEL ARBITRARY DEFORMATION-INDUCED ANISOTROPY*

R. M. BRANNON

Department of Computational Physics and Mechanics, Sandia National Laboratories, Albuquerque, NM 87185-0820

ABSTRACT

A unifying framework is developed for the analysis of brittle materials. Heretofore diverse classes of models result from different choices for unspecified coefficient and distribution functions in the unified theory. Material response is described in terms of expectation integrals of transverse symmetry tensors. First, a canonical body containing cracks of all the same orientation is argued to posses macroscopic transverse isotropy. An orthogonal basis for the linear subspace consisting of all double-symmetric transversely-isotropic fourth-order tensors associated with a given material vector is introduced and applied to deduce the explicit functional dependence of the compliance of such contrived materials on the shared crack orientation. A principle of superposition of strain rates is used to write the compliance for a more realistic material consisting of cracks of random size and orientation as an expectation integral of the transverse compliance for each orientation times the joint distribution function for the size and orientation. Utilizing an evolving (initially exponential) size-dependence in the joint distribution, the general theory gives unprecedented agreement with measurements of the dynamic response of alumina to impact loading, especially upon release where the calculations predict the development of considerable deformation-induced anisotropy, challenging the conventional notion of shocks as isotropic phenomena.

1. INTRODUCTION

This paper introduces several tools and viewpoints that may prove useful in the analysis of microcracked bodies. Rather than fixating on debatable details, we will concentrate on fundamental issues, developing a general framework from which different simplifying assumptions lead to seemingly disparate classes of models. While our discussion focuses on microcracks, the concepts seem applicable to other microstructures like voids, inclusions, reinforcing fibers, etc.

We begin in Section 2 by describing a canonical problem of a statistically uniform array of microcracks *all having the same orientation* embedded in an isotropic matrix material. There we introduce our fundamental premise that such a material should possess transverse isotropy; that is, one should be able to rotate this material about an axis parallel to the shared crack normal without affecting the fourth-order macroscopic compliance tensor. Our preliminary goal is to derive

*This work performed at Sandia National Laboratories supported by the Army Research Laboratory and the U.S. Department of Energy under contract DE-A-C04-94AL85000.

the explicit analytical dependence of the elastic compliance tensor on the shared crack normal. To this end, Section 3 introduces dual second-order projection tensors that decompose vectors into parts normal and transverse to the crack plane. We use these projection tensors to construct five fourth-order tensors that decompose second-order tensors into parts that are normal and transverse to the crack plane, as well as parts that shear the crack plane and parts that couple the transverse and normal components. We will demonstrate in Section 4 that our fourth-order decomposition tensors form a basis for the linear subspace of all fourth-order tensors that are transversely isotropic about a particular privileged direction. Hence, we argue in Section 5 that the compliance tensor for any material containing cracks of all the same orientation *must* be expressible as a linear combination of this basis. This result is very general because it follows only from our premise that such a material should be transversely isotropic. Physical considerations such as crack opening displacement or crack interactions affect only the *coefficient* functions — the basis itself is a pure function of crack orientation. This result may unify conflicting solutions in the literature by showing that they must all have the same fundamental structure, differing only in selected coefficient functions. Dienes' coefficient functions [1] presented in Section 6 utilize known small-distortion single-crack solutions to describe the extra strain that results when cracks open under applied tensile stress and when crack faces slide across each other under applied shearing stress.

The principal advantage of our transverse basis is that it is expressed in direct notation (i.e, the dependence on the shared crack normal is expressed algebraically), which permits us to extend the solution for same-orientation cracks to realistic crack patterns. As explained in Section 7, crack normals may be described by corresponding points on the unit sphere. In Section 8, we introduce a joint distribution function of crack size and orientation (position on the unit sphere) that describes the statistical variation in crack size and orientation observed in real materials. In applications, this function conditionally depends on spatial location (to account for, say, crack clustering) and time (to accommodate crack growth and nucleation). In Section 9, we integrate our same-size and same-orientation transversely-isotropic compliance tensor over the joint distribution, to

produce an expression for the *arbitrarily anisotropic* compliance of a realistic material.

The complete theory is tantamount to a *seven-dimensional* problem (four for space and time, one for crack size, and two for crack orientation). It may be simplified in any of several ways, depending on the class of problems to be solved. For example, one assumption described in Section 10 assumes crack size and orientation are independent random variables, allowing the size part of the distribution function to be modeled in detail for materials such as propellants where knowing crack surface area is important. If the material contains no predominant crack orientations, we show that the general anisotropic integral reduces to an *isotropic* compliance with the shear and bulk moduli expressed in terms of the unspecified transverse compliance coefficient functions. An alternative approach discussed in Section 11 assumes an analytical form (e.g., an evolving exponential) for the crack size dependence of the distribution function, thereby permitting analytical integration of the size part of the compliance integral. Here, to permit deformation-induced cracking in multiple directions, size and orientation are *not* assumed independent. For numerical implementations, the compliance integral is transformed into a sum by discretizing the unit sphere into contiguous groups of crack normals. A technique is discussed in Section 12 for avoiding "numerical healing" that can occur in Eulerian or rezoned calculations when conventional mixing rules assign inappropriately small crack sizes to mixtures. In Section 13, the tools developed in this paper are synthesized in numerical form to demonstrate excellent agreement with time-resolved uniaxial-strain shock wave experiments for aluminum oxide.

In summary, this paper educes fundamental mathematical results (such as explicit transverse dependence on crack orientation) while segregating arguable physical effects into unspecified material functions (the transverse coefficient functions and the joint size and orientation distribution). In this sense, we present here a flexible unifying viewpoint from which various choices of material functions lead to existing (heretofore disparate) classes of microcrack models.

2. A CANONICAL CRACKED BODY

Ultimately, we intend to deduce an expression for the compliance of an arbitrarily anisotropic cracked material. As a *starting point*, consider a material having a spatially uniform array of cracks all of a *given orientation*, **N** (left side of Figure 1). For small distortions, symmetry demands that the macroscopic material properties be unchanged upon any rigid rotation about **N**.

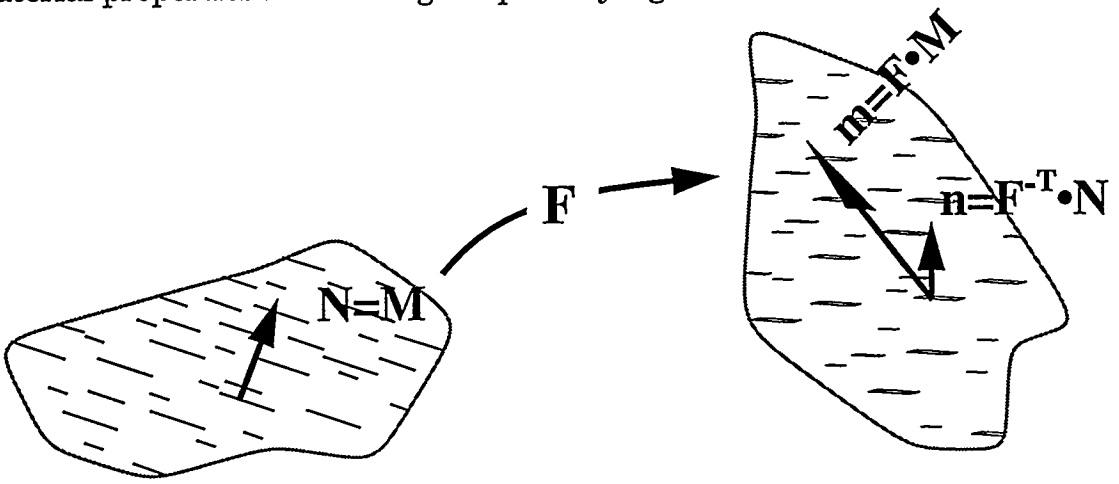

Figure 1: A body containing cracks all of the same orientation **N** subjected to a deformation **F**.

Figure 1 shows a material fiber **M** (i.e., a macroscopic conceptual line of material points) that was originally coincident with the unit crack normal **N**. If the vector **M** moves with the material, it will deform to an orientation parallel to

$$\mathbf{m} \equiv \mathbf{F} \bullet \mathbf{M} \,. \tag{2.1}$$

However, by Nanson's relation [2,3], the crack normal **N** deforms to a new orientation that is parallel to

$$\mathbf{n} \equiv \mathbf{F}^{-T} \bullet \mathbf{N} \,. \tag{2.2}$$

Neither **n** nor **m** are generally unit vectors, but since $\mathbf{n} \bullet \mathbf{m} = 1$, they serve as useful dual curvilinear base vectors. For small distortions, $\mathbf{n} \approx \mathbf{m}$. A general form for the compliance of this canonical cracked material will be derived in Section 5 by using the tensor decompositions discussed next.

3. DUAL PROJECTORS

Two vectors **m** and **n** are "dual" vectors if $\mathbf{n} \bullet \mathbf{m} = 1$. Consider a second-order projector **P** and its dual projector **Q**, defined by dyads between **m** and **n**:

$$P_{ij} = m_i n_j \tag{3.1a}$$

$$Q_{ij} = \delta_{ij} - m_i n_j \,. \tag{3.1b}$$

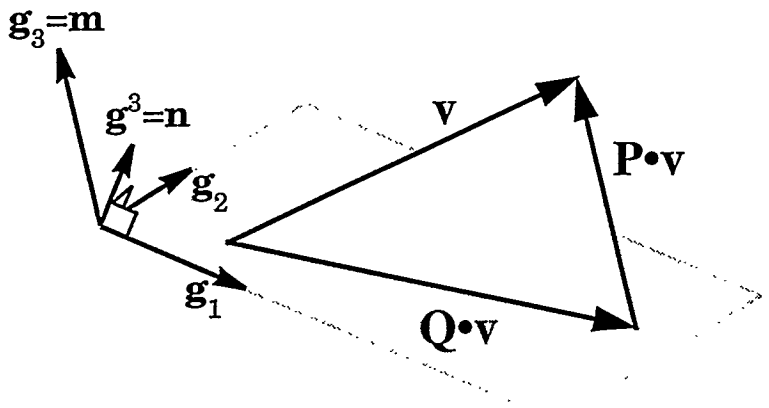

Figure 2: Decomposition of a vector **v** by the projectors **P** and **Q**. The projection **P•v** is parallel to **m**, and the projection **Q•v** is in the plane defined by **n**. For small distortions (**n≈m**), the projections are perpendicular and the projectors are symmetric dyads. For large distortions (**n≠m**), the projections are nonorthogonal and the projectors are nonsymmetric dyads. In either case, **P+Q=I** and **P•Q=Q•P=0**.

As illustrated in Figure 2, the projectors **P** and **Q** can be used to decompose vectors into parts in the direction of **m** and parts in the plane whose normal is parallel to **n**. Utilizing a curvilinear basis in which the base vector $\mathbf{g}_3 = \mathbf{m}$ and its dual $\mathbf{g}^3 = \mathbf{n}$, the actions of **P** and **Q** on any vector **v** are

$$\mathbf{P} \bullet \mathbf{v} = \mathbf{m}(\mathbf{n} \bullet \mathbf{v}) = \begin{Bmatrix} 0 \\ 0 \\ v^3 \end{Bmatrix}$$

$$\mathbf{Q} \bullet \mathbf{v} = \mathbf{v} - \mathbf{m}(\mathbf{n} \bullet \mathbf{v}) = \begin{Bmatrix} v^1 \\ v^2 \\ 0 \end{Bmatrix}. \tag{3.2}$$

Note that $\mathbf{P} \bullet \mathbf{v}$ is not perpendicular to $\mathbf{Q} \bullet \mathbf{v}$ except for small distortions.*

*The inner product cannot be computed by simply multiplying the two arrays in (3.2) since both of those arrays contain *contravariant* components.

Five useful operators $\{\mathbf{B}_1, \ldots, \mathbf{B}_5\}$ can be constructed using $\mathbf{P}$ and $\mathbf{Q}$ to similarly decompose any second-order tensor $\mathbf{A}$ into parts in the direction of $\mathbf{m}$ and in the plane defined by $\mathbf{n}$, as well as into shearing and coupled parts. Namely,

$$\mathbf{B}_1\!:\!\mathbf{A} \equiv \mathbf{P}(\mathbf{P}^T\!:\!\mathbf{A}) = \begin{bmatrix} 0 & 0 & 0 \\ 0 & 0 & 0 \\ 0 & 0 & A^3_{.3} \end{bmatrix} \tag{3.3a}$$

$$\mathbf{B}_2\!:\!\mathbf{A} \equiv \mathbf{Q}(\mathbf{Q}^T\!:\!\mathbf{A}) = \begin{bmatrix} A^1_{.1} & 0 & 0 \\ 0 & A^2_{.2} & 0 \\ 0 & 0 & 0 \end{bmatrix} \tag{3.3b}$$

$$\mathbf{B}_3\!:\!\mathbf{A} \equiv \mathbf{P}(\mathbf{Q}^T\!:\!\mathbf{A}) + \mathbf{Q}(\mathbf{P}^T\!:\!\mathbf{A}) = \begin{bmatrix} A^3_{.3} & 0 & 0 \\ 0 & A^3_{.3} & 0 \\ 0 & 0 & A^1_{.1} + A^2_{.2} \end{bmatrix} \tag{3.3c}$$

$$\mathbf{B}_4\!:\!\mathbf{A} \equiv \mathbf{P} \bullet \mathbf{A} \bullet \mathbf{Q} + \mathbf{Q} \bullet \mathbf{A} \bullet \mathbf{P} = \begin{bmatrix} 0 & 0 & A^1_{.3} \\ 0 & 0 & A^2_{.3} \\ A^3_{.1} & A^3_{.2} & 0 \end{bmatrix} \tag{3.3d}$$

$$\mathbf{B}_5\!:\!\mathbf{A} \equiv \mathbf{Q} \bullet \mathbf{A} \bullet \mathbf{Q} = \begin{bmatrix} A^1_{.1} & A^1_{.2} & 0 \\ A^2_{.1} & A^2_{.2} & 0 \\ 0 & 0 & 0 \end{bmatrix}. \tag{3.3e}$$

Existence of the fourth-order tensors $\{\mathbf{B}_1, \ldots, \mathbf{B}_5\}$ follows from the linearity of these operations. In fact, their components are:

$$(\mathbf{B}_1)_{ijkl} = P_{ij}P_{lk} \tag{3.4a}$$

$$(\mathbf{B}_2)_{ijkl} = Q_{ij}Q_{lk} \tag{3.4b}$$

$$(\mathbf{B}_3)_{ijkl} = P_{ij}Q_{lk} + Q_{ij}P_{lk} \tag{3.4c}$$

$$(\mathbf{B}_4)_{ijkl} = P_{ik}Q_{lj} + Q_{ik}P_{lj} \tag{3.4d}$$

$$(\mathbf{B}_5)_{ijkl} = Q_{ik}Q_{lj}\,. \tag{3.4e}$$

4. TRANSVERSE BASIS

Throughout the remainder of this work, we will use the projectors **P** and **Q** from taking **m=n=N**, where **N** is a material axis of symmetry that is not necessarily coincident with any of the three laboratory base vectors. Taking **m=n** does not restrict the discussion to small distortions if the constitutive laws are phrased in terms of the second Piola-Kirchhoff stress with Lagrange strain instead of the unrotated Cauchy stress with the unrotated rate of deformation [4].

Components of a vector or tensor with respect to a basis having the 3-direction aligned with **N** are "material components." The goal of this section is to deduce the laboratory components of transversely-isotropic tensors *without having to perform a coordinate transformation* between the material basis and the laboratory basis.

A symmetric second-order tensor **C** is transversely isotropic if $R_{pi}R_{qj}C_{ij} = C_{pq}$ for any rotation **R** about a material axis of symmetry **N**. The *material* matrix of such a tensor must be of the form

$$\mathbf{C} = \begin{bmatrix} c_q & 0 & 0 \\ 0 & c_q & 0 \\ 0 & 0 & c_p \end{bmatrix} . \tag{4.1}$$

where c_q and c_p are scalars. Direct expressions for such a tensor are

$$\mathbf{C} = c_p\mathbf{P} + c_q\mathbf{Q} \tag{4.2a}$$

$$C_{ij} = c_pN_iN_j + c_q(\delta_{ij} - N_iN_j) \ . \tag{4.2b}$$

These algebraic expressions are more useful than the material matrix (4.1) because they are easy to compute, integrate, and differentiate in the *laboratory* basis. For example, if only (4.1) were available, the simple operation $\mathbf{C} \bullet \mathbf{v}$ would require 21 multiplications because of the need to rotate to and from the material basis; with (4.2), the operation requires only 12 multiplications. Note from (4.2a) that **P** *and* **Q** *may be interpreted as second-order base tensors for the two-dimensional space of second-order tensors that are transversely isotropic about* **N**.

We now extend this concept to fourth-order tensors. A fourth-order tensor **H** is called "double-symmetric" if its rectangular Cartesian components satisfy $H_{ijkl} = H_{jikl} = H_{ijlk} = H_{klij}$. It is transversely isotropic with respect to a material

vector **N** if it is unchanged upon any rigid rotation **R** about **N** (i.e., $R_{pi}R_{qj}R_{rk}R_{sl}H_{ijkl} = H_{pqrs}$). The *material* Euclidean Voigt components (Appendix) of any double-symmetric transversely-isotropic tensor are of the form

$$\begin{bmatrix} H_{11} & H_{12} & H_{13} & 0 & 0 & 0 \\ H_{12} & H_{11} & H_{13} & 0 & 0 & 0 \\ H_{13} & H_{13} & H_{33} & 0 & 0 & 0 \\ 0 & 0 & 0 & H_{44} & 0 & 0 \\ 0 & 0 & 0 & 0 & H_{66} & 0 \\ 0 & 0 & 0 & 0 & 0 & H_{66} \end{bmatrix} \quad \text{with} \quad H_{11} = H_{44} + H_{12} \ . \tag{4.3}$$

When solving problems involving transverse symmetry, a typical approach is to simply set up a coordinate system aligned with the material directions. This approach becomes impractical when dealing with multiple transverse symmetries each having different axes. To later facilitate integration of a function of a transversely isotropic tensor, we seek a *direct* representation of (4.3). This goal is similar in spirit to our producing (4.2) as a useful direct representation of (4.1).

Just as **P** and **Q** were recognized as a direct basis for second-order transverse tensors, we now identify five fourth-order base tensors $\{\mathbf{B}_1,...,\mathbf{B}_5\}$ that span the space of all double-symmetric fourth-order tensors that are transversely isotropic with respect to a *particular* material vector **N**. Any linear combination of members of this space is itself a member of the space. Hence, there must exist a basis $\{\mathbf{B}_1,...,\mathbf{B}_5\}$ where, for any tensor **H** in the space, there exist scalars $\{h_1,...,h_5\}$ so that

$$\mathbf{H}(\mathbf{N}) = \sum_{k=1}^{5} h_K \mathbf{B}_K(\mathbf{N}) \ . \tag{4.4}$$

Applying minor symmetry to the five tensors in (3.4) gives just such a basis:

$$(\mathbf{B}_1)_{ijkl} = N_i N_j N_k N_l \tag{4.5a}$$

$$(\mathbf{B}_2)_{ijkl} = \delta_{ij}\delta_{kl} - N_i N_j \delta_{kl} - \delta_{ij} N_k N_l + N_i N_j N_k N_l \tag{4.5b}$$

$$(\mathbf{B}_3)_{ijkl} = N_i N_j \delta_{kl} + N_k N_l \delta_{ij} - 2N_i N_j N_k N_l \tag{4.5c}$$

$$(\mathbf{B}_4)_{ijkl} = \frac{1}{2}(N_i N_k \delta_{jl} + N_j N_l \delta_{ik} + N_i N_l \delta_{jk} + N_j N_k \delta_{il}) - 2N_i N_j N_k N_l \tag{4.5d}$$

$$\begin{aligned}(\mathbf{B}_5)_{ijkl} = {} & \delta_{ik}\delta_{jl} + \delta_{il}\delta_{jk} \\ & - (\delta_{ik} N_j N_l + \delta_{il} N_j N_k + \delta_{jk} N_i N_l + \delta_{jl} N_i N_k) \\ & + 2(N_i N_j N_k N_l) \ .\end{aligned} \tag{4.5e}$$

Equivalence with (4.3) follows by using (4.5) to write the material matrix of (4.4)

$$\begin{bmatrix} h_2+h_5 & h_2 & h_3 & 0 & 0 & 0 \\ h_2 & h_2+h_5 & h_3 & 0 & 0 & 0 \\ h_3 & h_3 & h_1 & 0 & 0 & 0 \\ 0 & 0 & 0 & h_5 & 0 & 0 \\ 0 & 0 & 0 & 0 & h_4 & 0 \\ 0 & 0 & 0 & 0 & 0 & h_4 \end{bmatrix} . \tag{4.6}$$

Note that the Euclidean Voigt components of any base tensor $\mathbf{B}_K$ in (4.5) can be determined from (4.6) by setting h_K=1 and all other h-coefficients to zero.

The component forms (4.5) are useful in practice because *they are algebraic (and easily integrable) functions of the privileged direction* **N**. They are, however, somewhat difficult to interpret physically. For conceptual discussions, observing how the basis (4.5) transforms tensors is far more revealing. The basis (4.5) decomposes second-order tensors (such as the stress) into normal, transverse, mixed, and coupled parts. Specifically, for any symmetric second-order tensor $\underline{\sigma}$,

$$\mathbf{B}_1:\underline{\sigma} = \begin{bmatrix} 0 & 0 & 0 \\ 0 & 0 & 0 \\ 0 & 0 & \sigma_{33} \end{bmatrix} \tag{4.7a}$$

$$\mathbf{B}_2:\underline{\sigma} = \begin{bmatrix} \sigma_{11}+\sigma_{22} & 0 & 0 \\ 0 & \sigma_{11}+\sigma_{22} & 0 \\ 0 & 0 & 0 \end{bmatrix} \tag{4.7b}$$

$$\mathbf{B}_3:\underline{\sigma} = \begin{bmatrix} \sigma_{33} & 0 & 0 \\ 0 & \sigma_{33} & 0 \\ 0 & 0 & \sigma_{11}+\sigma_{22} \end{bmatrix} \quad \leftarrow \textit{ not a projection} \tag{4.7c}$$

$$\mathbf{B}_4:\underline{\sigma} = \begin{bmatrix} 0 & 0 & \sigma_{13} \\ 0 & 0 & \sigma_{23} \\ \sigma_{31} & \sigma_{32} & 0 \end{bmatrix} \tag{4.7d}$$

$$\mathbf{B}_5:\underline{\sigma} = \begin{bmatrix} \sigma_{11} & \sigma_{12} & 0 \\ \sigma_{21} & \sigma_{22} & 0 \\ 0 & 0 & 0 \end{bmatrix}. \tag{4.7e}$$

The TI basis (4.5) is distinguished from so-called fabric tensors because it has nothing to do with material constants such as Poisson's ratio. It is a purely mathematical construct resulting from transverse symmetry only. Incidentally, the basis can be orthogonalized by replacing $\mathbf{B}_5$ by $\mathbf{B}_5 - \frac{1}{2}\mathbf{B}_2$ and $\mathbf{B}_2$ by $\frac{1}{2}\mathbf{B}_2$.

5. COMPLIANCE FOR SAME-ORIENTATION CRACKS

Our *preliminary* goal is to describe the macroscopic compliance for a material containing a statistically uniform array of cracks all having the *same orientation* and the *same size.* The compliance tensor $\mathbf{H}$ must surely be a function of crack size c, crack orientation $\mathbf{N}$, and the number of cracks per unit mass, $\tilde{N}$. Of course the compliance also must depend on the underlying matrix material properties, which we denote collectively as μ. The geometry of the crack distribution demands that the elastic compliance $\mathbf{H}$ for this material must be transversely isotropic. That is, it must be expressible as a linear combination of the basis (4.5):

Single crack size c and orientation N

$$\mathbf{H}(c, \mathbf{N}, \tilde{N}, \mu) = \mathbf{H}_m(\mu) + \mathbf{H}_c(c, \mathbf{N}, \tilde{N}, \mu) \,, \tag{5.1}$$

where

$$\mathbf{H}_c(c, \mathbf{N}, \tilde{N}, \mu) \equiv \sum_{k=1}^{5} \alpha_k(c, \tilde{N}, \mu)\mathbf{B}_k(\mathbf{N}) \,. \tag{5.2}$$

Here, $\mathbf{H}_m$ is the compliance of the underlying matrix material and $\mathbf{H}_c$ may be regarded as a compliance enhancement. The coefficients α_k depend on the crack size (distribution), the crack geometry, the number of cracks per unit mass, and the matrix elastic properties, but *not* on the crack orientation **N** (except to account for contact nonlinearities as noted in Section 6). Each $\mathbf{B}_K$, on the other hand, depends *only* on the orientation and is completely independent of any material properties. Thus, (5.1) shows the explicit form of dependence on orientation **N** in a direct notation expression. *The general form (5.1) follows only from the symmetry principle that an isotropic material containing a uniform array of same-orientation cracks must possess macroscopic transverse symmetry.* It is therefore a very general result.

The expression (5.1) purposely avoids adopting any *particular* form for the five α_K coefficient functions. Different researchers may derive different — even contradictory — expressions for the compliance of a body having same-orientation cracks. However, all admissible expressions for the compliance of an array of same-orientation cracks *must* be expressible in the form (5.1). They will differ only in the specific forms chosen or derived for the five coefficient functions $\alpha_K(c, \tilde{N}, \mu)$.

6. DIENES' α_K COEFFICIENTS.

Microcracks can increase the elastic compliance (decrease the stiffness) of a material. Closed cracks in compression do not affect the compliance perpendicular to their planes, whereas open cracks do. Therefore, the compliance is greater in tension than in compression. Closed cracks subjected to large normal compression may be locked by friction at the crack faces and do not affect the shear compliance. On the other hand, if the normal compression is low enough, the crack faces may slip, thereby increasing the compliance for shear in the plane of the crack.

Incorporating these concepts with analytical results for single tensile cracks, Dienes [1] applies the principle of superposition of strain rates to derive a closed-form solution for the compliance associated with open cracks. Dienes also provides a similar derivation using solutions for single shear cracks. In the current notation, Dienes' expression is a *special case* of the very general form (5.1) and can be shown to correspond to the following values for the crack coefficients:

$$\alpha_1 = \frac{8(1-\nu_m)}{3\mu_m} c^3 \rho_o \tilde{N} \quad \{\eta\} \tag{6.1a}$$

$$\alpha_4 = \frac{8(1-\nu_m)}{3\mu_m(2-\nu_m)} c^3 \rho_o \tilde{N} \quad \{\eta + (1-\eta) f_s\} \tag{6.1b}$$

$$\alpha_2 = \alpha_3 = \alpha_5 = 0 \tag{6.2c}$$

where ν_m is Poisson's ratio for the matrix material, μ_m is the shear modulus for the matrix material, and $\rho_o \tilde{N}$ is the number of cracks per unit reference *volume*. The quantities in braces account for "contact nonlinearities." The parameter η is defined to equal 1 if the crack is open and 0 if it is closed in compression. The factor

$$f_s \equiv Max\left(0 \ , 1 - \bar{\mu} \sqrt{\frac{\underset{\sim}{\sigma}:\mathbf{B}_1:\underset{\sim}{\sigma}}{\frac{1}{2}\underset{\sim}{\sigma}:\mathbf{B}_4:\underset{\sim}{\sigma}}}\right). \tag{6.3}$$

is a compliance-reducing factor that accounts for friction at the crack faces ($\bar{\mu}$ is the static or dynamic coefficient of friction, depending on whether the crack faces are in relative motion). The roles of η and f_s become more clear if (6.1) is applied and (4.7) are used in (5.1) to give the following explicit expression for elastic strain $\underset{\sim}{\varepsilon}^e$ as a function of stress $\underset{\sim}{\sigma}$:

$$\underset{\sim}{\varepsilon}^e = \mathbf{H}:\underset{\sim}{\sigma}$$

$$= \mathbf{H}_m:\underset{\sim}{\sigma} + \alpha_1\mathbf{B}_1:\underset{\sim}{\sigma} + \alpha_4\mathbf{B}_4:\underset{\sim}{\sigma}$$

$$= [\underset{\sim}{\varepsilon}^e_m] + \alpha_1\begin{bmatrix}0&0&0\\0&0&0\\0&0&\sigma_{33}\end{bmatrix} + \alpha_4\begin{bmatrix}0&0&\sigma_{13}\\0&0&\sigma_{23}\\\sigma_{31}&\sigma_{32}&0\end{bmatrix}. \qquad (6.4)$$

The first term, $\underset{\sim}{\varepsilon}^e_m$, is the strain that would result from the applied stress if the material were free of cracks. The second term represents *additional* strain in the 33-direction that results whenever there exists a 33 component of stress that tends to open the cracks. Recalling the definition of the coefficient α_1, observe that this extra strain occurs only when the cracks are open (η=1), not when they are closed in compression (η=0). Contact nonlinearities make the coefficients (6.1) depend on the crack orientation because η is usually determined by the sign of $\mathbf{N}\bullet\underset{\sim}{\sigma}\bullet\mathbf{N}$. Likewise, the expression (6.3) involves the crack normal. The third term in (6.4) represents additional shearing strain caused by shearing stresses in the plane of the cracks. The crack is said to be "locked" if the applied shear stress is not large enough to overcome the nominal friction stress. If a crack is locked, relative motion of the crack faces cannot occur, and there must be no shear compliance enhancement (i.e., $\alpha_4 = 0$). This requirement is accommodated by the "*Max*" operation in (6.3). Whenever the cracks are closed but not locked, the friction factor f_s reduces the applied shear stress by the amount of friction present.

Dienes (and many others) neglect the extra *lateral* strain that would be caused by an *axial* stress, even though this contribution may become increasingly significant as large cracks open up. Noting that σ_{33} appears in the 11 and 22 positions in (4.7c), capturing this effect requires a non-zero coefficient of the base tensor $\mathbf{B}_3$ (which, incidentally, is the only one not proportional to a projector).

We now introduce some tools that will allow us to extend the general equation (5.1) for the compliance of a body containing same-size and same-orientation cracks to a realistic body having cracks of many sizes and many orientations.

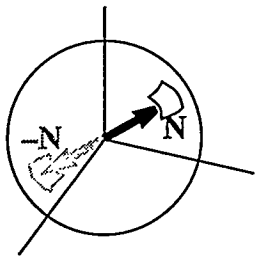

Figure 3: Unit normals map to the unit sphere. The union of diametrically opposite areas represents a solid angle.

7. ORIENTATION AND THE UNIT SPHERE

Crack orientation is described by the unit normal **N** to the crack plane or, alternatively, by corresponding points on the unit sphere (Fig 3). For example, the unit normal **N**={1,0,0} corresponds to the point (1,0,0) on the sphere. For *cracks*, diametrically opposite points on the unit sphere are equivalent. Put differently, any constitutive function $f(\mathbf{N})$ should have the property that $f(-\mathbf{N})=f(\mathbf{N})$. By using the unit sphere, any function of **N** may be regarded as a function on the unit sphere. Any contiguous *set* of crack normals may be described by a contiguous patch of area on the unit sphere together with the diametrical image of that area. Such a union of areas is hereafter referred to as a "**solid angle**".

8. JOINT PROBABILITY DISTRIBUTION $P(C,\mathbf{N})$

Real materials do not contain same-size same-orientation cracks. Consider a body of *unit mass* containing a *total* of $\tilde{N}$ cracks. In a realistic model, a randomly selected crack could have any orientation **N** and any size c (usually taken to be the radius). As with oil shale or partially spalled metal, some sizes and some orientations may be more common than others. This variation is described through the use of a **joint distribution function**, $p(c,\mathbf{N})$, defined by its interpretation when integrated:

> The probability that a randomly selected crack will have a size that lies between a and b and will have an orientation **N** that lies in some solid angle $\Delta\Omega$ on the unit sphere is given by
>
> $$\int_{\Delta\Omega}\int_{a}^{b} p(c,\mathbf{N})\,dc\,d\Omega \ . \qquad (8.1)$$

The function $p(c,\mathbf{N})$ might conditionally depend on the spatial location of the randomly selected crack. Since cracks nucleate, grow, and coalesce, $p(c,\mathbf{N})$ is also implicitly a function of time. Of course, the integral over all possible crack sizes and orientations (i.e. over the entire unit sphere and from c=0 to ∞) is unity.

If a randomly selected crack is *known* to have an orientation **N**, then the probability it has a size that lies between a and b is given by

$$\int_a^b p(c \mid \mathbf{N})\, dc \ , \tag{8.2}$$

where the *conditional* distribution $p(c \mid \mathbf{N})$ is defined

$$p(c \mid \mathbf{N}) \equiv \frac{p(c, \mathbf{N})}{\int_0^\infty p(c, \mathbf{N})\, dc} \ . \tag{8.3}$$

Surprisingly, joint and conditional distributions are rarely encountered in the literature. Instead, researchers often present more intuitive and more easily measured **number density plots** like the one sketched in figure 4 where the total number of cracks (per volume) exceeding size c is plotted as a function of c. *Number density plots must never have a positive slope.*

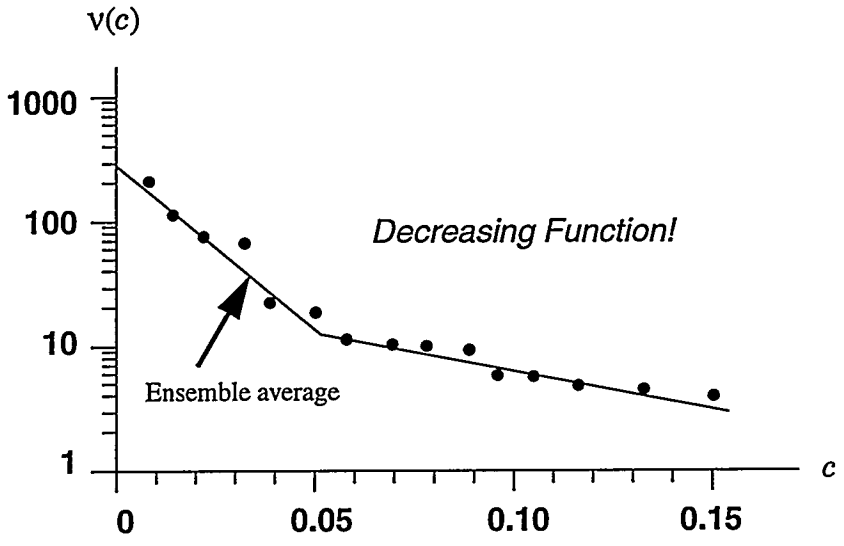

Figure 4: An intuitive and popular way to display crack size distribution information, $\nu(c)$ is the number of cracks (usually of some particular orientation N) per unit volume exceeding size c. Thus, the vertical intercept is the total number of cracks per unit volume. In practice, this intercept is determined by extrapolating an ensemble average (solid line) from the smallest measured crack size.

A number density function $\nu(c)$ may be converted to a probability function by simply dividing it by the total number of cracks, $\nu(0)$. This normalized function

$\nu(c)/\nu(0)$ is the probability that a randomly selected crack will have a size exceeding c. Thus, the relationship between a number density plot and the joint distribution function is

$$\boxed{p(c \mid \mathbf{N}) = -\frac{1}{\nu(0)}\left(\frac{\partial \nu}{\partial c}\right)_{\mathbf{N}}} \quad . \tag{8.4}$$

The size and orientation distribution function $p(c,\mathbf{N})$ will now be combined with the compliance (5.1) for same-size same-orientation cracks to derive the compliance for a body containing cracks of many sizes and orientations.

9. COMPLIANCE FOR RANDOM-SIZE RANDOM-ORIENTATION CRACKS

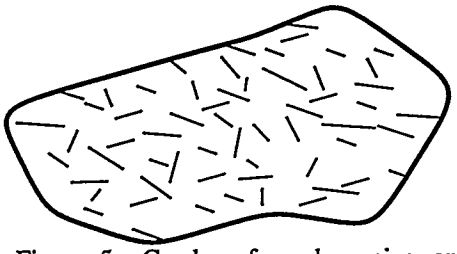

Figure 5: Cracks of random size and random orientation.

Consider a body containing an array of random size and orientation cracks (Fig 5). Applying a principle of superposition of strain rates for a dilute array of cracks, the increase in compliance is taken to be the sum of the increases for each possible crack size and orientation times the number of cracks of that specified size and orientation. For a continuous distribution of crack sizes, the compliance $\mathbf{H}$ is computed by the expectation integral

$$\mathbf{H} = \int_{\Omega}\int_{0}^{\infty} \mathbf{H}(c, \mathbf{N}, \tilde{N}, \mu) p(c, \mathbf{N})\, dc\, d\Omega \quad , \tag{9.1}$$

where $\mathbf{H}(c, \mathbf{N}, \tilde{N}, \mu)$ is given by (5.1). For nondilute arrays of cracks, it seems reasonable to expect the compliance to nevertheless be of the above form, with the dependence on $\tilde{N}$ being nonlinear to account for crack interaction. With (5.1), the expression (9.1) may be alternatively written

$$\boxed{\mathbf{H} = \mathbf{H}_m + \sum_{k=1}^{5} \int_{\Omega} \mathbf{B}_k(\mathbf{N})\, \bar{\alpha}_k(\mathbf{N}, \ldots) d\Omega} \quad , \tag{9.2}$$

where $\bar{\alpha}_k(\mathbf{N}, \ldots)$ is the *orientation-dependent* expected value of α_k, a function of the crack density and the material properties as well as the crack orientation:

$$\bar{\alpha}_k(\mathbf{N}, \tilde{N}, \mu) \equiv \int_0^\infty \alpha_k(c, \mathbf{N}, \tilde{N}, \mu) p(c, \mathbf{N}) dc \quad . \tag{9.3}$$

10. ORIENTATION DISTRIBUTION ASSUMPTION (ISOTROPIC MODEL)

Evaluating (9.2) with modest computing resources would certainly require simplifying assumptions, depending on the salient features one wishes to capture. In the next few subsections, we will explore some simplifying assumptions, defining the class of problems for which each is sensible.

One simplification assumes a particular form for the joint distribution that leads to an isotropic crack model. This assumption and its consequences are presented to provide a more meaningful background to the arbitrarily anisotropic model described later. For propellants and explosives, knowing the free surface area (from open crack faces) is of supreme importance, so capturing the crack *size* distribution may be more important than capturing *orientation* anisotropy. One (debatable) approach is to assume crack size and crack orientation are *independent* random variables, in which case,

$$p(c, \mathbf{N}) = g(c)h(\mathbf{N}) \quad , \tag{10.1}$$

where g and h are independent size and orientation distribution functions. Suppose it is further assumed that the cracks have no preferred orientations. Then the orientation distribution is uniform; that is, $h(\mathbf{N}) = 1/\Omega$, where Ω is the area of the unit sphere (4π). With these assumptions, (9.2) becomes

$$\mathbf{H} = \mathbf{H}_m + \sum_{k=1}^{5} \bar{\alpha}_k \bar{\mathbf{B}}_k \quad , \tag{10.2}$$

where $\bar{\alpha}_k$ is the expected value of $\alpha_k(c, \ldots)$, defined

$$\bar{\alpha}_k = \int_0^\infty \alpha_k(c, \ldots) g(c) dc \,, \tag{10.3}$$

and $\bar{\mathbf{B}}_k$ is the average of $\mathbf{B}_k(\mathbf{N})$ over all possible orientations (i.e., the average over the unit sphere):

$$\bar{\mathbf{B}}_k = \frac{1}{\Omega} \int_\Omega \mathbf{B}_k(\mathbf{N}) d\Omega \,. \tag{10.4}$$

It is straightforward (though tedious) to show that these averages are

$$\bar{\mathbf{B}}_1 = \frac{1}{3}\mathbf{P}^{sp} + \frac{2}{15}\mathbf{P}^{dev} \tag{10.5a}$$

$$\bar{\mathbf{B}}_2 = \frac{4}{3}\mathbf{P}^{sp} + \frac{2}{15}\mathbf{P}^{dev} \tag{10.5b}$$

$$\bar{\mathbf{B}}_3 = \frac{4}{3}\mathbf{P}^{sp} - \frac{4}{15}\mathbf{P}^{dev} \tag{10.5c}$$

$$\bar{\mathbf{B}}_4 = \frac{0}{3}\mathbf{P}^{sp} + \frac{6}{15}\mathbf{P}^{dev} \tag{10.5d}$$

$$\bar{\mathbf{B}}_5 = \frac{2}{3}\mathbf{P}^{sp} + \frac{7}{15}\mathbf{P}^{dev} \,. \tag{10.5e}$$

where $\mathbf{P}^{sp}$ and $\mathbf{P}^{dev}$ are the fourth-order spherical and symmetry-deviator projectors:

$$(\mathbf{P}^{sp})_{ijkl} = \frac{1}{3}\delta_{ij}\delta_{kl} \tag{10.6a}$$

$$(\mathbf{P}^{dev})_{ijkl} = \frac{1}{2}(\delta_{ik}\delta_{jl} + \delta_{il}\delta_{jk}) - \frac{1}{3}\delta_{ij}\delta_{kl} \,. \tag{10.6b}$$

When $\mathbf{P}^{dev}$ operates on a second order tensor, the result is the symmetric deviatoric part of the tensor, but $\mathbf{P}^{dev}$ *itself* is an *isotropic* fourth-order tensor, as is $\mathbf{P}^{sp}$. Hence, substituting (10.5) into (10.2) gives an *isotropic* compliance

$$\mathbf{H} = \frac{1}{2\mu}\mathbf{P}^{dev} + \frac{1}{3K}\mathbf{P}^{sp} \,. \tag{10.7}$$

where effective shear and bulk moduli μ and K are given by

$$\frac{1}{\mu} = \frac{1}{\mu_m} + \frac{2}{15}(2\bar{\alpha}_1 + 2\bar{\alpha}_2 - 4\bar{\alpha}_3 + 6\bar{\alpha}_4 + 7\bar{\alpha}_5) \tag{10.8a}$$

$$\frac{1}{K} = \frac{1}{K_m} + \bar{\alpha}_1 + 4\bar{\alpha}_2 + 4\bar{\alpha}_3 + 2\bar{\alpha}_5 \ . \tag{10.8b}$$

If the expressions in (6.1) are used, (10.8) becomes

$$\frac{\mu_m}{\mu} = 1 + \frac{32(5-\nu_m)(1-\nu_m)}{45(2-\nu_m)} \rho_o \tilde{N} \overline{c^3} \tag{10.9a}$$

$$\frac{K_m}{K} = 1 + \frac{16(1-\nu_m^2)}{9(1-2\nu_m)} \rho_o \tilde{N} \overline{c^3} \ . \tag{10.9b}$$

The quantity $\overline{c^3}$ is the expected value of crack size cubed (quite different from the cube of the expected value of crack size). The *dimensionless* quantity $\rho_o \tilde{N} \overline{c^3}$ is the so-called *crack volume*, seen often in the literature.

A clever *anisotropic* extension used in current BFRACT theory [5] employs the above approach until one particular crack orientation, is considered to dominate the material anisotropy. This critical orientation is determined by monitoring, say, the maximum principal stress. Thereafter, the orientation distribution would effectively contain a Dirac delta function.

11. SIZE DISTRIBUTION ASSUMPTION (ANISOTROPIC MODEL)

The preceding isotropic and dominant crack approaches fail to accurately model cracks in shear. Hot spots created by local shearing at crack faces may be responsible for early ignition of certain propellants. Furthermore, even for problems such as spall that do indeed involve one dominant crack direction, cracks of other orientations (usually at angles ~45 degrees from the dominant direction) tend to grow in shear *prior* to the development of a dominant crack. Finally, problems involving significant *redirections* of the applied stresses inherently lead to multiaxial deformation-induced anisotropy.

The Los Alamos SCRAM code [6] is effectively a fully-anisotropic general implementation of Eqs. (9.2) and (6.1) together with conventional high-pressure equations of state and flow models not discussed in this paper. This base coding was extensively modified to run using Sandia's Eulerian shock physics code CTH

[7] (it was actually modified to comply with new model packaging standards [8] that permit it to run on *any* parent code).

To model arbitrary deformation-induced anisotropy, crack size and crack orientation are *not* assumed independent. Dienes [1] assumes a general analytical form for the c-dependence of $p(c, \mathbf{N})$ that — in effect — permits the integral in (9.3) to be solved *a priori* to give $\bar{\alpha}_k(\mathbf{N})$ in closed form, eliminating the need to numerically store, evolve, and integrate the c-dependent part of the distribution. (Alternative analytical size distributions will be explored in later work.)

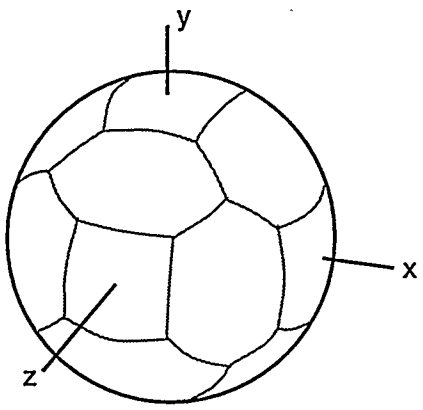

Figure 6: (a) A nine bin discretization of the unit sphere. Of the 18 discretized areas, only half represent distinct bin directions.

With $\bar{\alpha}_k(\mathbf{N})$ known and $\mathbf{B}_k(\mathbf{N})$ given by (4.5), all that remains (to compute the compliance) is to perform the integral (9.2) over all possible crack orientations by discretizing the area of the unit sphere into a finite set of patches, called *"bins"*. The nine-bin discretization in Figure 6 is used most often in our calculations because it is coarse enough to be computationally tractable, but fine enough to capture considerable anisotropy. Three-bin and even one-bin discretizations are useful for rapid set-up computations. A one-bin solution is roughly equivalent to the approach of Section 10.

Our Sandia-SCM code approximates each $\bar{\alpha}_k(\mathbf{N})$ as piecewise constant over the unit sphere so that (9.2) becomes

$$\mathbf{H} = \mathbf{H}_m + \sum_{k=1}^{5} \sum_{b=1}^{n_b} \tilde{\alpha}_{kb} \tilde{\mathbf{B}}_{kb} \Delta\Omega_b \quad . \tag{11.1}$$

where $\Delta\Omega_b$ is the *solid angle* for bin b (i.e., the union of diametrically opposite areas on the sphere), n_b is the number of bins, and

$$\tilde{\mathbf{B}}_{kb} \equiv \frac{1}{\Delta\Omega_b} \int_{\Omega_b} \mathbf{B}_k d\Omega \quad . \tag{11.2}$$

and $\tilde{\alpha}_{kb}$ is the piecewise constant value of $\bar{\alpha}_k(\mathbf{N})$ for bin b. Since a crack of orientation $-\mathbf{N}$ is equivalent to a crack of orientation $\mathbf{N}$, the dependence on $\mathbf{N}$ is really a dependence on the projector $\mathbf{P}$ in (3.1) with $\mathbf{m}=\mathbf{n}=\mathbf{N}$. Thus, Sandia-SCM uses

$$\tilde{\alpha}_{kb} = \bar{\alpha}_k(\tilde{\mathbf{P}}_b) \,, \tag{11.3}$$

where $\tilde{\mathbf{P}}_b$ may be regarded as the *centroid* of the bin, namely,

$$\tilde{\mathbf{P}}_b \equiv \frac{1}{\Delta\Omega_b} \int_{\Delta\Omega_b} \mathbf{P} d\Omega \quad . \tag{11.4}$$

To appreciate the importance of using this average of projectors over each bin, consider the radically coarse discretization of the unit sphere into only one single bin. It is straightforward to show that for one bin, $\tilde{\mathbf{P}}$ is just 1/3 of the identity tensor. Thus, for example, if $\bar{\alpha}_k(\mathbf{N})$ depends on the normal component of traction, $\mathbf{N} \bullet \underset{\sim}{\sigma} \bullet \mathbf{N} = \underset{\sim}{\sigma}:\mathbf{P}$, its approximation will use a "good guess" for the normal component of traction, namely,

$$\underset{\sim}{\sigma}:\tilde{\mathbf{P}} = \frac{1}{3} tr \underset{\sim}{\sigma} \,. \tag{11.5}$$

Recall that each $\mathbf{B}_k$ is a function of $\mathbf{N}$ *only*. Therefore, the integrals in (11.2) are independent of the material and problem geometry and may be computed *a priori*. In Sandia-SCM, these integrals have been computed numerically for 1-, 3-, and 9-bin discretizations and are hard-wired in the numerical coding.

By discretizing the unit sphere we allow orientation-dependence of the coefficient and distribution functions and associated arbitrary anisotropy. We conclude this section by defining a *scalar measure of anisotropy*. Any minor-symmetric fourth-order isotropic tensor may be expressed as a linear combination of $\mathbf{P}^{dev}$ and $\mathbf{P}^{sp}$ defined in (10.6). The isotropic part $\mathbf{H}^{iso}$ of any minor-symmetric fourth-order tensor $\mathbf{H}$ is the projection of $\mathbf{H}$ onto the linear manifold defined by the span of $\mathbf{P}^{dev}$ and $\mathbf{P}^{sp}$; that is,

$$\mathbf{H}^{iso} = (\mathbf{H}::\mathbf{P}^{sp})\mathbf{P}^{sp} + \frac{1}{5}(\mathbf{H}::\mathbf{P}^{dev})\mathbf{P}^{dev} \,. \tag{11.6}$$

Here, the symbol "::" denotes the fourth-order inner product (e.g., $\mathbf{A}::\mathbf{B} = A_{ijkl}B_{ijkl}$).The divisor of 5 in the second term is present because the Euclidean magnitude of $\mathbf{P}^{dev}$ is $\sqrt{5}$. If $\mathbf{H}$ is stored as a Euclidean Voigt matrix (see Appendix), the coefficients in (11.6) are computed as follows:

$$\mathbf{H}::\mathbf{P}^{sp} = \frac{1}{3}\left(\sum_{K=1}^{3}\sum_{L=1}^{3} H_{KL}\right) \tag{11.7a}$$

$$\mathbf{H}::\mathbf{P}^{dev} = \left(\sum_{K=1}^{6} H_{KK}\right) - \mathbf{H}::\mathbf{P}^{sp} \tag{11.7b}$$

The deviatoric part of the tensor $\mathbf{H}$ is just

$$\mathbf{H}' = \mathbf{H} - \mathbf{H}^{iso} \tag{11.8}$$

An anisotropy measure $\mathcal{A}$ is here defined in terms of the ratio of the deviatoric to isotropic magnitudes:

$$\mathcal{A} \equiv \frac{2}{\pi}\ \text{atan}\sqrt{\frac{\mathbf{H}' :: \mathbf{H}'}{\mathbf{H}^{iso} :: \mathbf{H}^{iso}}} \tag{11.9}$$

This quantitative measure of anisotropy goes from zero for an isotropic fourth-order tensor ($\mathbf{H} = \mathbf{H}^{iso}$) to unity for a deviatoric fourth-order tensor ($\mathbf{H} = \mathbf{H}'$).

Following a brief discussion of numerical issues for Eulerian codes, the fully anisotropic compliance (11.1) will be applied to a ceramic shock-wave experiment in Section 13, where we predict deformation-induced anisotropies in excess of 60%.

12. Healing in Eulerian/Rezone Calculations

Implementations of microcrack models are often plagued by "numerical healing" that occurs when mixing different states of damage (e.g., during rezoning of a Lagrangian mesh or during simple Eulerian advection). If each component i has a mass m_i and contains $\tilde{N}_i$ cracks per unit mass, the number of cracks per unit mass for the mixture is naturally

$$\tilde{N}_{mix} = \frac{\sum_i \tilde{N}_i m_i}{\sum_i m_i} \,. \tag{12.1}$$

When a material containing very small cracks is to be mixed with the same material containing large cracks, the effective crack size of the mixture must not be assigned using a simple volume- or mass-weighted average of the disparate crack sizes. To avoid numerical healing, the larger and/or more populated crack sizes must dominate. Sandia-SCM uses a number-weighted p-norm to assign a crack size to the mixture:

$$c_{mix} = \left(\frac{\sum_i c_i^p \tilde{N}_i m_i}{\sum_i \tilde{N}_i m_i} \right)^{1/p} \,. \tag{12.2}$$

where c_i is the average crack size of the ith component. To avoid numerical healing, p must be chosen larger than unity. The Dienes compliance coefficients (6.1) all depend on the expected value of crack size *cubed*. Therefore, to ensure a good mixture value for the elastic compliance, Sandia-SCM uses p=3. To avoid having to write special-purpose advection routines, Sandia-SCM advects the quantity $c_i^3 \tilde{N}_i m_i$ using the standard mass-weighted advection built into CTH.

13. Application to a Ceramic Shock-Wave Experiment

Figure 7 shows a sketch of the configuration for symmetric impact of AD995 aluminum oxide [9]. The velocity at the ceramic-window interface was measured using VISAR interferometry for impact speeds of 0.544 and 1.943 km/s.

Figure 8 shows good agreement of the Eulerian Sandia-SCM calculations with the experimental results, especially during the release phase, validating the techniques of Sections 11 and 12 using Eq. (6.1) in (9.2). The Lagrangian SCRAM code [6] — on which Sandia-SCM is based — produced similar results.

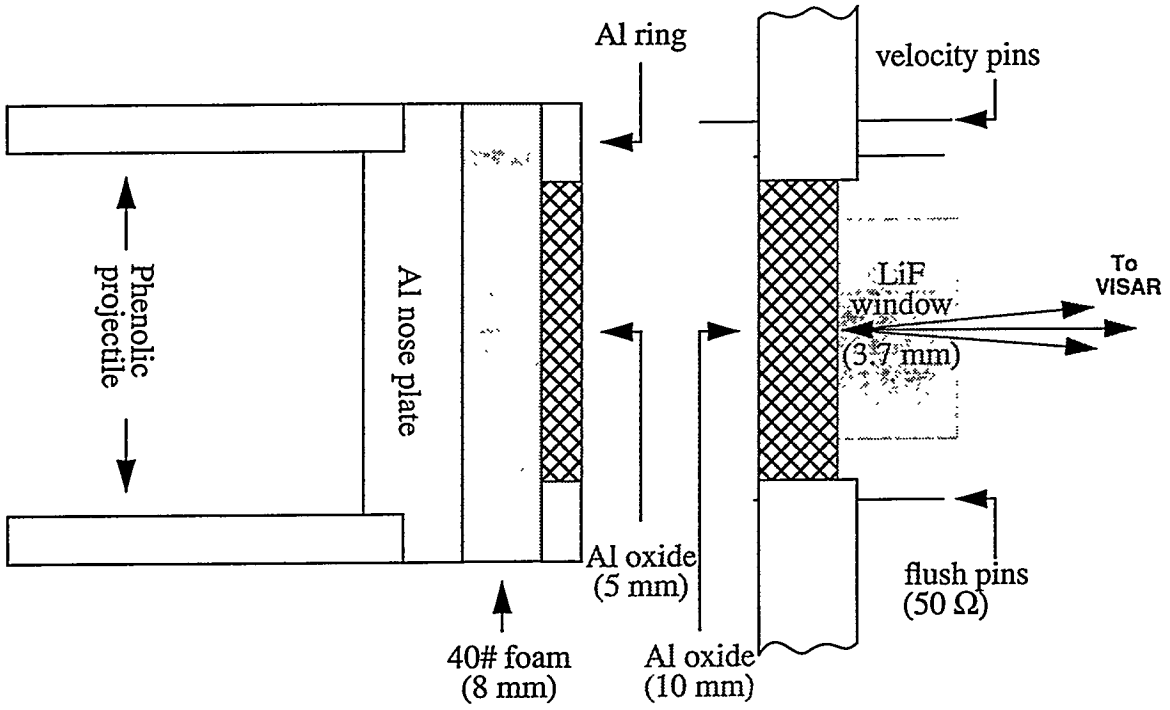

Figure 7: Experiment configuration for ceramic impact experiments.

The maximum computed deformation-induced anisotropy (see Eq. 11.9) for the lower-speed impact was about 4% during the loading phase and 56% by the end of the calculation. For the higher-speed impact, 3% anisotropy occurred during loading and 60% by the end of the calculation. For both calculations, the moderate anisotropy developed during loading (i.e., while the material was still in compression) was due to the growth of cracks in shear. This loading anisotropy was lower for the high-speed experiment because greater confining pressure resulted in greater friction at the crack faces, thereby inhibiting crack growth and slip. The high final anisotropies were due to catastrophic growth of cracks in tension. These results challenge the conventional view of shocks as isotropic phenomena. While simpler isotropic models can describe the loading part of the response reasonably well, only our *anisotropic* calculation has achieved good agreement for the release part of the response. Many other results from these calculations will be detailed in a separate paper, where we will also explain our means of determining material constants.

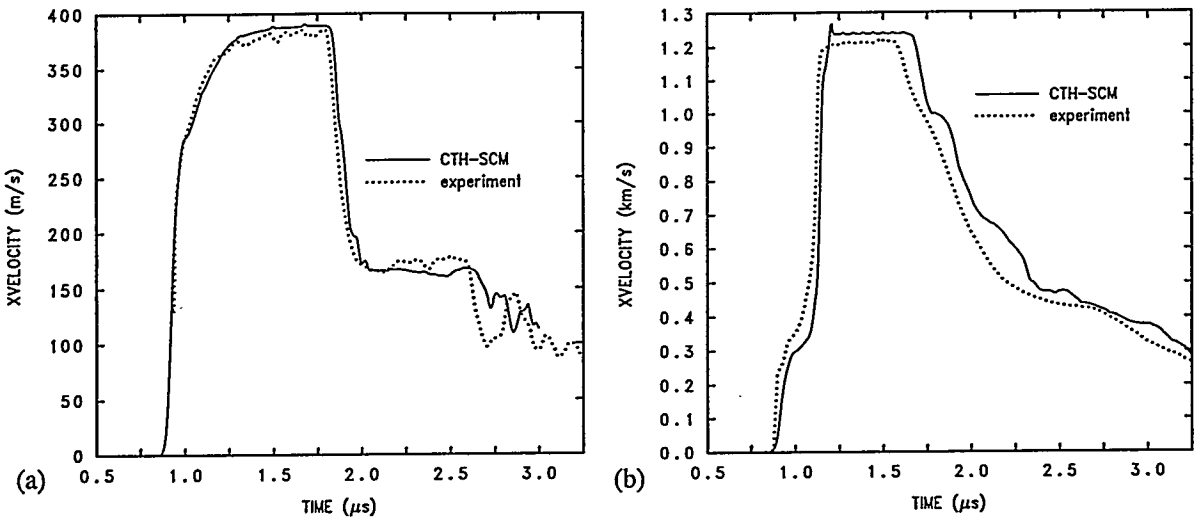

Figure 8: Comparison of theory and experiment for symmetric impact of aluminum oxide at impact speeds of (a) 0.544 and (b) 1.943 km/s. Both calculations used identical input data.

14. CONCLUSIONS

Many microcrack modeling techniques in the literature can be viewed as different aspects of the viewpoint presented in this work. Depending on the physical phenomena of interest, some models accurately predict the development of crack surface area at the expense of accurate predictions of anisotropy, and vice-versa for other models. The current work unifies these diverse viewpoints by explicitly showing the analytical dependence of a material's elastic compliance on crack size and crack orientation. We purposely segregated debatable aspects of our theory into *six* developer-defined material functions. The coefficient functions α_4 and α_1 in Eq. (5.2) describe additional strain caused by crack shearing and opening stresses, respectively. The often negligible coefficients α_2 and α_5 permit description of changes in transverse compliance due to the presence of cracks. The coefficient function α_3 allows description of *lateral* compliance increases associated with *axial* loads that may be important for large open cracks. The fifth and final developer-definable function, $p(c, \mathbf{N})$, describes the statistical distribution of crack sizes and crack orientations within a material. We showed how different choices for these six material functions lead to very different material models. For the anisotropic material functions, we defined a scalar

measure of anisotropy to *quantitatively* describe the important role of multi-directional cracking and deformation-induced anisotropy in one-dimensional shock wave experiments, thereby challenging the traditional notion that shock waves are principally isotropic phenomena.

15. REFERENCES

[1]J.K. Dienes, *Theory of Deformation: Part 2, Physical Theory.* Los Alamos National Laboratory report LA-11063-MS, Vol. II., 1989.

[2]Malvern, L. E., **Introduction to the Mechanics of a Continuous Medium**, Prentice-Hall Inc., Englewood Cliffs, N. J. (1969).

[3]J.K. Dienes, *Theory of Deformation: Part 1, Kinematics.* Los Alamos National Laboratory report LA-11063-MS, Vol. I., 1987.

[4]R. M. Brannon, *Frame indifference is not enough.* Submitted to: Acta Mechanica (1996).

[5]Seaman, L., Curran, D.R., Murri, W.J., *A Continuum Model for Dynamic Tensile Microfracture and Fragmentation*. Journal of Applied Mechanics 107, 1985.

[6]J.K. Dienes, *Theory of Deformation: Part 3, SCRAM: A Code for the Dynamic Response of Materials with Finite Deformation, Plastic Flow, and Microcracking.* Los Alamos National Laboratory report, 1994 in progress.

[7]J.M. McGlaun, S.L. Thomson, and M.G. Elrick, *CTH: A three-dimensional shock wave physics code.* Int. J. Impact Engr. Vol 10, No. 1-4, pp. 351-360 (1990).

[8]Brannon, R. M., *Model interface guidelines (MIG): rules for packaging models in a form that accelerates installation into any compliant code.* Sandia National Laboratories unpublished report.

[9]Grady, D.E., and Moody, R. L., *Shock Compression Profiles in Ceramics.* Sandia National Laboratories Technical Report SAND96-0551. 1996.

APPENDIX
EUCLIDEAN-VOIGT COMPONENTS

It is sporadically recognized among researchers that storing symmetric tensors using six-component Voigt arrays *with the off-diagonal components multiplied by* $\sqrt{2}$ results in a *Euclidean* inner-product rule. The factor of $\sqrt{2}$ is here rigorously justified by showing that it arises from a Euclidean (orthonormal) basis for the linear space, $\mathcal{V}$, of all symmetric second-order tensors (in $\mathcal{R}^3$). Since

any linear combination of tensors in $\mathcal{V}$ is itself in $\mathcal{V}$, there must exist an orthonormal basis of six tensors for $\mathcal{V}$. One such basis is

$$\mathbf{b}_1 = \mathbf{e}_1 \otimes \mathbf{e}_1 \tag{A.1a}$$

$$\mathbf{b}_2 = \mathbf{e}_2 \otimes \mathbf{e}_2 \tag{A.1b}$$

$$\mathbf{b}_3 = \mathbf{e}_3 \otimes \mathbf{e}_3 \tag{A.1c}$$

$$\mathbf{b}_4 = (\mathbf{e}_1 \otimes \mathbf{e}_2 + \mathbf{e}_2 \otimes \mathbf{e}_1)/\sqrt{2} \tag{A.1d}$$

$$\mathbf{b}_5 = (\mathbf{e}_2 \otimes \mathbf{e}_3 + \mathbf{e}_3 \otimes \mathbf{e}_2)/\sqrt{2} \tag{A.1e}$$

$$\mathbf{b}_6 = (\mathbf{e}_3 \otimes \mathbf{e}_1 + \mathbf{e}_1 \otimes \mathbf{e}_3)/\sqrt{2}\,, \tag{A.1f}$$

where $\{\mathbf{e}_1, \mathbf{e}_2, \mathbf{e}_3\}$ are the usual orthonormal base vectors for 3-dimensional laboratory space, and $\otimes$ denotes dyadic multiplication. The divisors of $\sqrt{2}$ ensure

$$\mathbf{b}_K : \mathbf{b}_J = \delta_{KJ}\,, \tag{A.2}$$

making this basis Euclidean. The double-dot product (:) is the second-order inner product (i.e, for any second-order tensors **A** and **B**, $\mathbf{A}:\mathbf{B}=A_{ij}B_{ij}$, where repeated lower-case indices are summed from 1 to 3).

Any symmetric second-order tensor **A** may be written as a *six-dimensional* Euclidean vector,

$$\mathbf{A} = \sum_{K=1}^{6} A_K \mathbf{b}_K\,. \tag{A.3}$$

The 6-dimensional vector components A_K are related to the usual 3-dimensional double-index second-order tensor components A_{ij} by

$$A_K = \mathbf{A}:\mathbf{b}_K = A_{ij}\mathbf{e}_i \otimes \mathbf{e}_j : \mathbf{b}_K, \text{ or}$$
$$\{A_1, A_2, A_3, A_4, A_5, A_6\} = \{A_{11}, A_{22}, A_{33}, \sqrt{2}A_{12}, \sqrt{2}A_{23}, \sqrt{2}A_{31}\}\,. \tag{A.4}$$

We call these the "*Euclidean* Voigt components" because the array is identical to the conventional Voigt representation of a symmetric second-order tensor *except for the very important factors of* $\sqrt{2}$. Incidentally, we order the trailing off-diagonal components {..., 12, 23, 31} contrary to "missing index" {..., 23, 31, 12} convention because 2-D calculations are usually performed in the 1-2 plane. Placing the zero 23 and 31 components at the end allows truncation to only four components, and

certain fourth-order tensor inverses may be performed on only the upper 4×4 submatrix.

Any minor-symmetric fourth-order tensor **U** (i.e., $U_{ijkl} = U_{jikl} = U_{ijlk}$) may be written as a second-order tensor in this 6-dimensional Euclidean space as

$$\mathbf{U} = \sum_{K=1}^{6} \sum_{M=1}^{6} U_{KM} \; \mathbf{b}_K \otimes \mathbf{b}_M \; . \tag{A.5}$$

The 6×6 matrix $[U_{KM}]$ for fourth-order minor-symmetric tensors is the same as the usual Voigt matrix except the last three rows and the last three columns are multiplied by $\sqrt{2}$ (thus, the lower-right 3×3 submatrix is multiplied by 2). For example, $U_{62} = \sqrt{2}\, U_{3122}$ and $U_{45} = 2\, U_{1223}$.

The basis (A.1) allows us to utilize Euclidean space theorems and properties. For example, the inner product **A:B**, which is ordinarily computed as $A_{ij}B_{ij}$, may be computed using the usual Euclidean rule

$$\mathbf{A}:\mathbf{B} = \sum_{K=1}^{6} A_K B_K \; . \tag{A.6}$$

Fourth-order operations are also performed in the familiar way. For example,

$$\mathbf{A}:\mathbf{U}:\mathbf{B} = \sum_{K=1}^{6} \sum_{M=1}^{6} A_K U_{KM} B_M \; . \tag{A.7}$$

The Euclidean components of the inverse of a fourth-order tensor are just the matrix inverse of the tensor's Euclidean Voigt components. If *conventional* non-Euclidean Voigt representations (i.e., *without* the factors of $\sqrt{2}$) had been used, these computations would be complicated by factors of 2 and 4, inhibiting efficient use of optimized Euclidean subroutines or intrinsic functions.

Euclidean Voigt components are not limited to symmetric tensors. The basis (A.1) can be augmented with three more base tensors consisting of normalized skew-symmetric dyads, $(\mathbf{e}_2 \otimes \mathbf{e}_1 - \mathbf{e}_1 \otimes \mathbf{e}_2)/\sqrt{2}$ etc., thereby spanning *all* second-order tensors in symmetric and skew-symmetric parts.

DISCLAIMER